ELSEVIER

International Journal of Mass Spectrometry 212 (2001) 519–533

www.elsevier.com/locate/ijms

Surface-induced dissociation

Optimization of a matrix-assisted laser desorption ionization-ion mobility-surface-induced dissociation-orthogonal-time-of-flight mass spectrometer: simultaneous acquisition of multiple correlated MS^1 and MS^2 spectra

Earle G. Stone, Kent J. Gillig, Brandon T. Ruotolo, David H. Russell*

The Laboratory for Biological Mass Spectrometry, Texas A&M University, Department of Chemistry, College Station, Texas 77843

Received 18 May 2001; accepted 1 August 2001

Abstract

Optimization of a matrix-assisted laser desorption ionization-ion mobility-surface-induced dissociation-o-time-of-flight mass spectrometer for peptide sequencing is discussed. Surface-induced dissociation (SID) spectra obtained by using stainless steel, Au grids, and fluorinated self-assembled monolayers (F-SAM) on Au are compared. The F-SAM surfaces yield similar fragment ions to those obtained using an adventitious hydrocarbon coated stainless steel surface; however, optimum collision energies differ for the two surfaces. The advantage of ion mobility-time-of-flight (TOF) is the ability to simultaneously acquire MS^1 and MS^2 spectra, which greatly facilitates high-throughput sequencing of peptides and mixtures of peptides resulting form the proteolytic digest of proteins. Simultaneous acquisition of ion mobility and TOF spectra introduces a time element to SID experiments that can be used as a probe of ion/surface interactions. (Int J Mass Spectrom 212 (2001) 519–533) © 2001 Elsevier Science B.V.

Keywords: Matrix-assisted laser desorption; Time-of-flight; Orthogonal

1. Introduction

The expanding need for protein identification and characterization (e.g. proteomics) has resulted in the development of more rapid, efficient mass spectrometry techniques to replace current methodologies [1–4]. Rapid growth in the field of biological mass spectrometry and especially the area of proteomics can be directly attributed to the development of ionization sources capable of introducing large, thermally labile molecules into the gas phase (i.e. matrix-assisted laser desorption ionization (MALDI) and electrospray ionization (ESI))[5]. The combination of MALDI or ESI with enzymatic digestion has proved to be a powerful tool for rapid identification of proteins; providing information that takes effective

* Corresponding author. E-mail: russell@mail.chem.tamu.edu

Dedicated to R. Graham Cooks on the occasion of his sixtieth birthday.

PII S1387-3806(01)00513-9

advantage of the extensive protein databases already in existence [6–8]. Identification of proteins that are not listed in a database or that are post-translationally modified may not be possible using only peptide mass mapping and tandem mass spectrometry provides an attractive, logical solution for such protein identifications [9,10].

Since the introduction of MALDI and ESI, the instrumentation used for tandem mass spectrometry (MS/MS) has undergone substantial changes. For example, the original tandem mass spectrometers were either triple quadrupoles or sector instruments [11]; but in the last few years MS/MS instruments such as quadrupole ion traps, reflectron time-of-flight (TOF), and various hybrid TOF instruments have been developed [12–14]. Typically the mass spectrometer (MS^1) is scanned to acquire the mass spectrum of the intact analytes, and MS^1 is used to select specific ions of interest. The mass selected ions are then fragmented using collision-induced dissociation (CID) [15], photodissociation [16], spontaneous decay (metastable ions) [17], or surface-induced dissociation (SID)[18], and the fragment ion spectra of the selected ion is acquired using a second mass spectrometer (MS^2). The primary limitation to this approach is the necessity of interrogating each intact analyte ion individually by scanning electric or magnetic fields, thus limiting sample throughput of complex mixtures. The simultaneous acquisition of all product ions from a mixture of analytes has been demonstrated using Fourier transform-ion cyclotron resonance (FTICR) multiplexing schemes [19]. However, the information obtained is limited by the lack of a correlation between the MS^2 ions and precursor $[M+H]^+$ ions.

In a previous paper we described a MALDI ion mobility-TOF instrument that is well suited for high throughput analysis, and the advantages of MALDI coupled to IM-TOF MS were discussed [12]. In this paper we expand the utility of the IM-TOF experiment to include SID for purposes of peptide sequencing. Briefly, MALDI is a pulsed ionization method ($\sim$5 ns pulse width), thus the ions are formed over a very short time span, and predominately singly charged $[M+H]^+$ ions with relatively low internal energies are formed [20–24]. The pulsed nature of the MALDI-IM experiment provides a new dimension to fundamental studies of SID. For example, time based studies applied to SID experiment can reveal differences between ions undergoing quasi-elastic scattering, inelastic scattering, or capture and thermal desorption providing insight to the partitioning of translational energy into the three post-collision modes; conversion to internal energy, transfer to the surface, and scattering energy. Additionally, Denisov and coworkers have noticed dramatic improvement in signal to noise for their FTICR SID studies, which is important for biological samples where often the signal of interest is one for a peptide of low counts or may be lost in the biological, or matrix background [25]. The sensitivity of MALDI for peptides is excellent, as it exhibits both low detection limits (femtomole and subfemtomole) [26–28], and a relatively high tolerance of contaminants commonly found in biological samples (salts, buffers, detergents, etc.). Additionally, the utility of MALDI as a high-pressure ionization method has been demonstrated previously [29,30]. The use of MALDI is even more appealing for high throughput protein analysis in light of the recent developments in sample preparation such as Zip Tips™ coupled with MALDI [31–33].

Ion mobility (IM) can be used to separate gas phase ions on the basis of collision cross-section-to-charge ratio, Ω/z [34,35]. The time to separate ions on the basis of IM require milliseconds to seconds depending upon total length of the drift cell, the gas pressure, the applied drift voltage, and the size of the ion. Thus, it is possible to design an instrument such that the IM drift time is very short, e.g. hundreds of microseconds to milliseconds, but much greater than the time required (10–100 microseconds) to acquire a TOF mass spectrum. This is important because this permits signal averaging of the TOF mass spectrum as the ions elute the drift cell. As the IM separated $[M+H]^+$ ions undergo activation in a field free region of the instrument, both $[M+H]^+$ ions and fragment ions arrive in the TOF ion source at the same time, which correlates the fragment ions to a specific precursor ion [36,37].

Our selection of SID as a means of ion activation

for IM-TOF MS was based on several factors. Primary among these are instrumental cost and simplicity. For example, IM drift tubes and TOF analyzers are relatively simple to design and construct, and SID does not require expensive lasers for photodissociation nor introduction of a bath gas for CID. Significant progress has been made in the last few years to better understand SID and to improve reliability as a structural probe for gas-phase ions [18]. Although the combination of IM with CID has been demonstrated previously [38], it is unclear how changes in the ion's velocity that accompanies collisional activation [15,39,40] influence calibration of the fragment ion spectra. On the other hand, SID is a single impulsive collision excitation event and ion-surface interactions should not significantly alter the drift time correlation between precursor and fragment ions. That is, the precursor and fragment ions leave the surface with a common, narrow velocity distribution, thus arrival time of the ions in the TOF ion source should be the same [18,41].

In this paper we describe our attempts to optimize MALDI-IM-SID for the analysis of biomolecules. Specifically, optimization of surface conditions is discussed in light of both preliminary data and our most recent results using fluorinated self-assembled monolayers (F-SAM). Such surfaces have been shown to retain their chemical purity and to be more efficient for producing SID fragment ions [42]. Surface choice is of particular importance in the context of an IM-SID experiment, and this point is discussed in detail.

2. Experimental

The samples used for these studies, the peptides RKEVY [molecular weight (MW) 693.81], des-Arg^9 bradykinin (AA sequence RPPGFSPF, MW 904.05), bradykinin (AA sequence RPPGFSPFR, MW 1060.24), gramicidin S (AA sequence cyclo-LFPVOLFPVO, MW 1141.5), substance P (AA sequence RPKPQQFFGLM-NH_2, MW 1346.6), and α-melanocyte stimulating hormone (α-MSH) (AA sequence Ac-SYMEHFRWGK PV-NH_2, MW 1664.9), were purchased from Sigma (St Louis, Missouri) and used as delivered upon mixing 1 mg per 1 mL of methanol. All samples were then prepared by diluting 2 μL of the peptide solution with 20 μL of a matrix solution composed of 11 mg of α-cyano-4-hydroxycinnamic acid and 11 mg of fructose in 1 mL of methanol. 2–4 μL of the analyte/matrix solution, corresponding to a few hundred picomoles of material, were deposited by the dried droplet method onto the direct insertion probe tip.

Spectra were obtained for RKEVY, bradykinin, and des-Arg^9 bradykinin using a hydrocarbon coated (adventitious pump oil) gold grid (Buckbee-Mears, St. Paul, Minnesota) in-line (perpendicular to the ion beam) between the mobility drift cell and the extraction plates of the o-TOF source with a drift cell length of 4 cm (See Fig. 1 inset A) [12]. For these experiments two grids, 300 lines per inch, 90% transmittance, were overlaid to reduce the transparency to ~80%. This design was chosen based on convenience for performing SID in-line.

SID was also accomplished using an adventitious hydrocarbon coated stainless steel surface or an F-SAM (Fig. 1) [42,43]. These surfaces were positioned 40° to the incident ion beam and 1 cm directly below a gridded TOF extraction plate (angled plate drawn in Fig. 1). This is similar to the early instrument configuration employed by Bier and coworkers [44]. Further instrument changes are needed to optimize the instrument and will include both improved pre-SID ion optics and some post-SID ion optics to enhance the quality of the spectra presented here. Also the length of the drift cell was increased to 29.5 cm. The instrument was further modified to allow the movement (see arrow Fig. 1) of the 20 cm o-TOF such that the SID surface could be lowered out of the ion beam and allow the acquisition of non-SID spectra (Fig. 1 Inset B.)

MALDI was performed in the IM drift cell (Fig. 1) at a pressure of 5–10 Torr helium using a 337 nm nitrogen laser operated at near-threshold desorption levels with a repetition rate of 20 Hz. Ultra high purity helium was purchased from Praxair (Danbury, Connecticut) and used without further purification or drying. The total IM drift cell voltage was between 1500 and 1750 V, 5–12 V cm^{-1} Torr^{-1}. SID incident

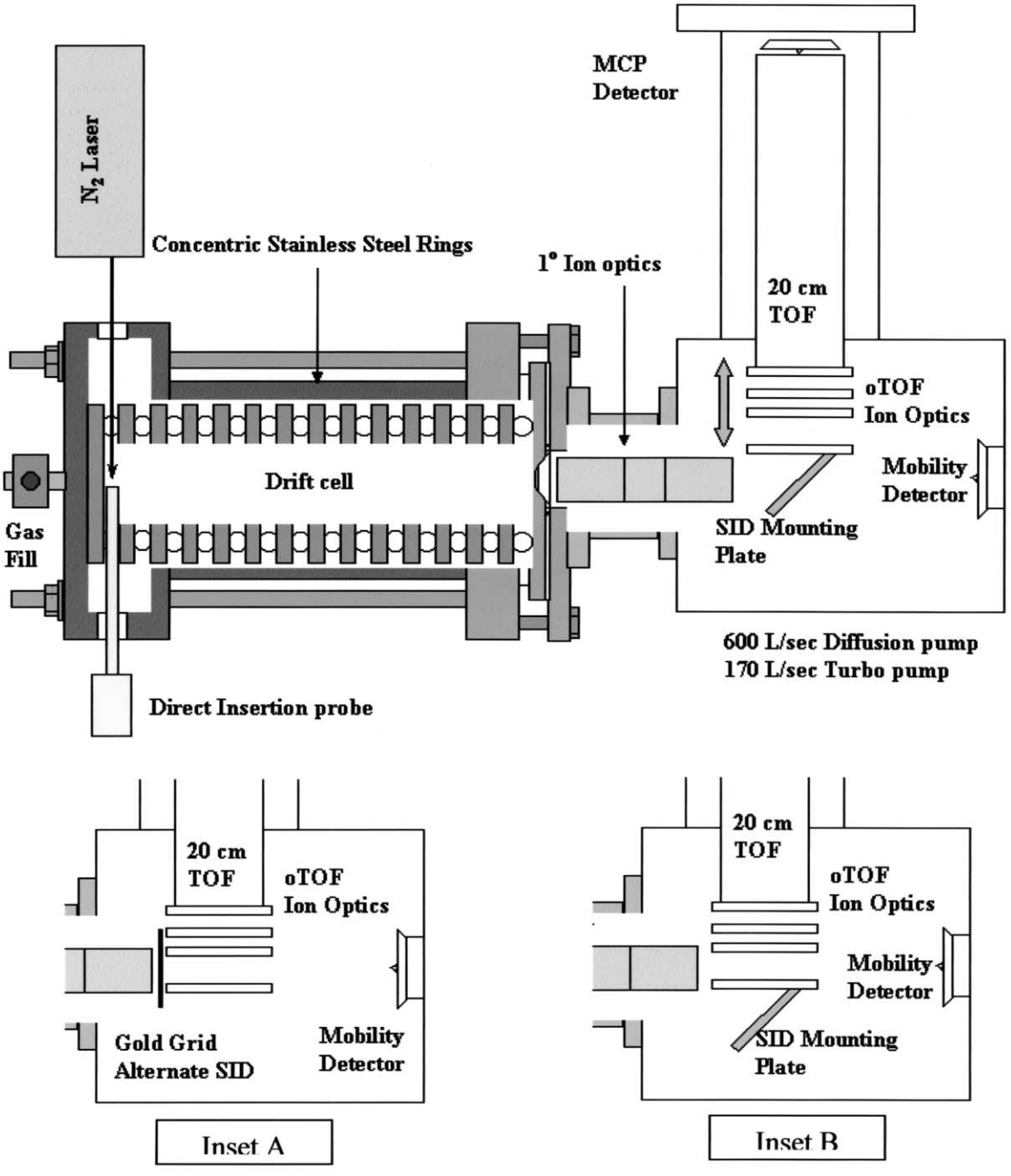

Fig. 1. A cutaway drawing of the MALDI-IM-SID-o-TOF mass spectrometer used in these experiments. Inset A shows the instrument configuration used to perform the gold grid SID experiments. Inset B shows the current instrument configuration in non-SID mode.

energies, 20–100 eV, were adjusted using the primary ion optics with the extraction plate bias voltages adjusted to optimize mass resolution [m/Δm, full width at half maximum (FWHM)]. The mass resolution for non-SID fragment ions was greater than 200 and decreased to less than 100 for SID experiments. Therefore the $[M+H]^+$ and $[M+Na]^+$ ions are not completely resolved and the SID spectra could contain fragment ions from both species. We do not detect abundant fragment ions in the SID spectra that we would expect for the $[M+Na]^+$ precursor ions, and this is probably due to the higher activation energies required to fragment the adduct ions. Data was acquired for 1–2 min. The 20 cm TOF, pulser electronics, time-to-digital converter (TDC)/timer card, and data acquisition software were provided by Ionwerks (Houston, Texas). Data analysis was accomplished using Grams/32 (Thermo Galactic, Salem, New Hampshire) or Fortner Transform Version 3.3 (Research Systems, Boulder, Colorado) software packages. Fortner Transform was used to generate two-dimensional contour plots with mobility separation shown as total drift time on the y-axis, *m/z* information shown on the x-axis, and brighter colors, yellow to white, indicating higher ion counts (hereafter denoted as a mass-mobility plot). The data acquired using the Ionwerks TDC was smoothed for all contour plots.

3. Results and discussion

The following sections describe a series of experiments aimed at optimizing the MALDI-IM-SID-TOF-MS experiment. The combination of IM and TOF for SID studies provides considerable flexibility in terms of instrument design. To a first approximation the drift time for an ion through a high-pressure gas is proportional to its volume (size) [45]. However, subtle changes in drift time can occur as a result of small volume changes, i.e. intramolecular interactions [46]. Thus, IM and TOF are used as time-domain *m/z* separators, and fragment ions arising from protonated peptides that dissociate following mobility separation arrive in the time-of-flight ion source simultaneously establishing a drift-time correlation between the fragment ions and the precursor $[M+H]^+$ ion. The *m/z* value of $[M+H]^+$ and fragment ions are then measured using the TOF analyzer. The resulting plot of mobility drift time vs. *m/z* (TOF) yields both a series of mobility separated $[M+H]^+$ ions (the peptide mass map) and the fragment ion spectra associated with a particular $[M+H]^+$ ion (peptide sequence information) [36,37].

4. Preliminary results

Figs. 2–4 contain SID spectra acquired using adventitious hydrocarbon coated gold grids. See Fig. 1, inset A for details concerning positioning of the grids. These spectra were recorded using collision energies of approximately 20 eV. The spectrum (Fig. 2) of RKEVY contains a complete series of a-, b-, and y-type fragment ions as well as signals for the loss of small neutral molecules such as H_2O and NH_3 from many of the fragment ions. A complete set of a-, b-, and y-type fragment ions are also observed for des-Arg^9 bradykinin (Fig. 3), with the exception of fragment ions resulting from cleavage of the pro-gly amide bond (a_3, b_3, and y_5 ions). The spectrum of bradykinin (Fig. 4) is very similar to that for des-Arg^9 bradykinin, and fragment ions resulting from cleavage of the pro-gly amide bond (a_3, b_3, and y_6 ions) are also absent. The absence of fragment ions resulting from cleavage of the pro-gly amide bond contradicts suggestions that proline lowers the bond dissociation energy for the adjacent amide backbone bond [47]. The apparent contradiction is probably a result of stabilizing interaction between the N-terminal arginine and the C-terminus, [48–50] rather than some underlying feature related to the surface activation process.

5. Optimization of instrumental design

To increase the resolution and transmission efficiency of IM we designed and constructed a longer, periodic focusing drift cell [51]. Fig. 5 contains a

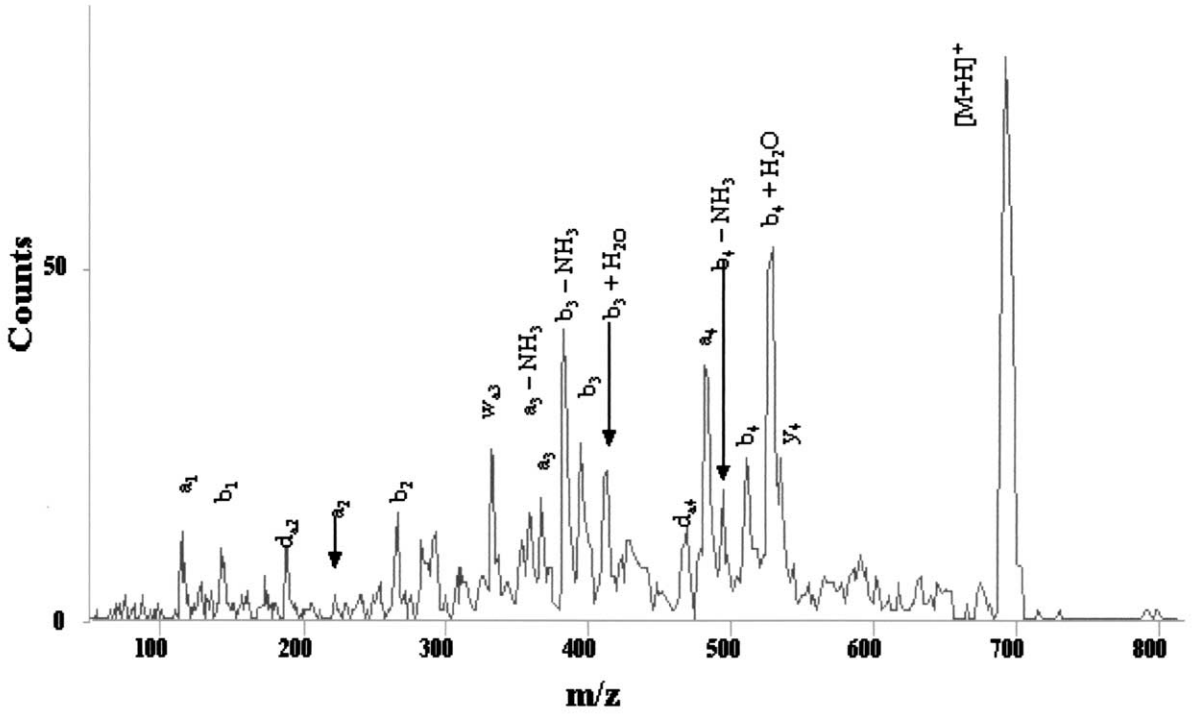

Fig. 2. A MALDI-IM-SID-o-TOF mass spectrum of the pentapeptide RKEVY. This spectrum was acquired using the gold grid arrangement in Fig. 1 Inset A. Data was acquired for 2 min and analyzed using GRAMS/32. Mass resolution, m/ΔM at FWHM, is better than 200. Mobility resolution is better than 20.

mass-mobility plot of a mixture of five peptides composed of des-Arg^9 bradykinin, bradykinin, gramicidin S, substance P, and α-MSH. A mobility resolution of 50–75 was obtained using the new drift cell as compared to 20–30 for a conventional IM drift cell. The data shown in Fig. 5 was acquired using near-threshold MALDI laser fluence, which primarily yields $[M+H]^+$ or $[M+Na]^+$ ions. The gramicidin S $[M+Na]^+$ ion is observed as a weak signal with a slightly longer drift time and higher *m/z* relative to the $[M+H]^+$ ion signal. Note that a plot of drift time vs. *m/z* yields a near-linear correlation for structurally related compounds [36]. For example, the slopes, hereafter denoted as "trend-lines", for matrix ions is very different from that for peptide $[M+H]^+$ ions [52]. The near-linear mass-mobility relationship provides the basis for using IM as MS^1 in the MS-MS mode [36].

The mass-mobility plot is also used to correlate the fragment ions to their respective precursor ions. That is, fragment ions that are formed after the precursor ions elute the drift cell have the same apparent drift time as the precursor ion. On the other hand, fragment ions that are formed upon ionization appear at a drift time characteristic of that ion, and fragment ions that are formed during the time the ions are drifting through the drift cell have a broad, ill-defined arrival time distribution. The lack of observable fragment ions in Fig. 5 demonstrate that the $[M+H]^+$ ions elute from the drift cell without excess internal energies.

6. Optimization of parameters affecting ion mobility-time-of-flight tandem mass spectrometry

Fig. 6 contains an SID mode mass-mobility plot for a five peptide mixture using an adventitious hydrocarbon coated stainless steel surface, positioned as

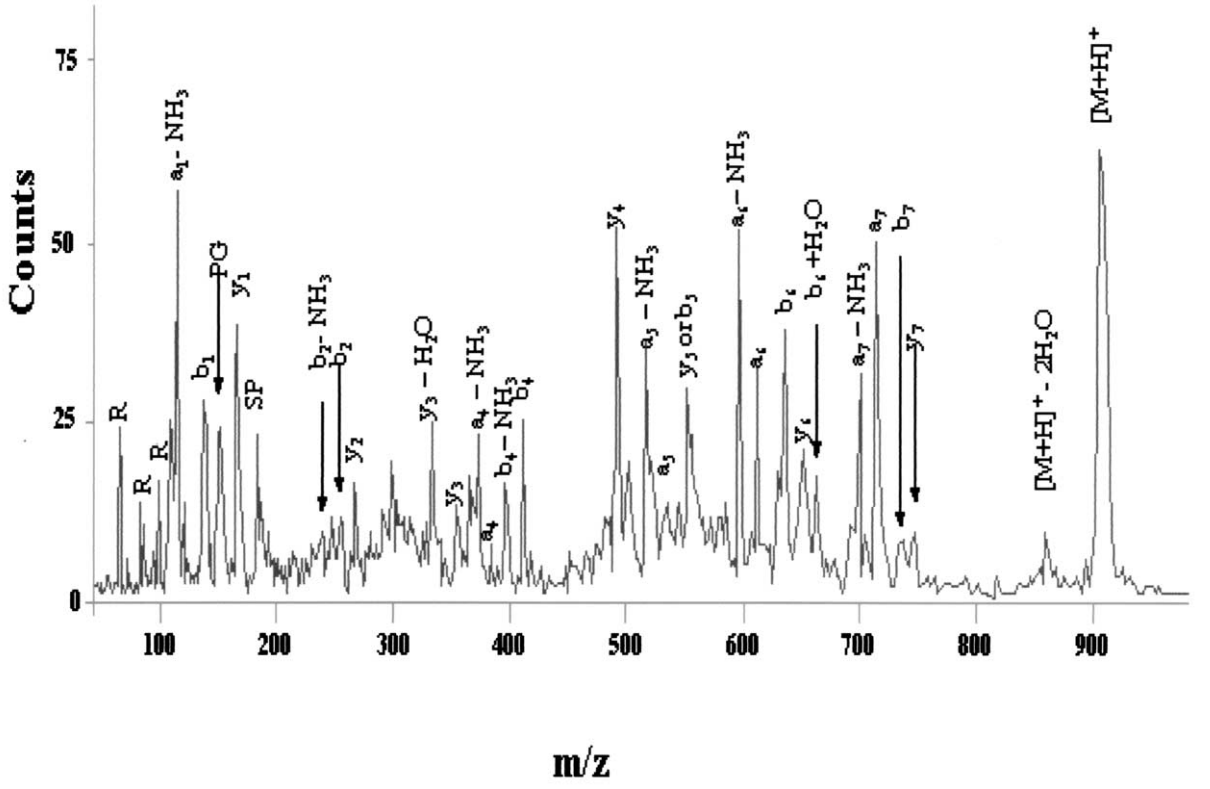

Fig. 3. A MALDI-IM-SID-o-TOF mass spectrum of des-Arg^9 bradykinin. This spectrum was acquired using the gold grid arrangement in Fig. 1, Inset A. Data was acquired for 2 min and analyzed using GRAMS/32. Mass resolution, m/ΔM at FWHM, is better than 200. Mobility resolution is better than 20.

shown in Fig. 1, at 90 eV collision energy. Fragment yields using the surface positioned 40° to the extraction plates of the TOF were much higher (a minimum of an order of magnitude higher) when compared to the fragment yields of the in-line arrangement. The increased fragmentation efficiency (intensity of ions observed) is primarily attributed to the fact that all ions must impact the surface for the surface positioned 40° to the mass spectrometer whereas as much as 80% of the ion beam in the in-line experiments may not have collided with the gold mesh. Four of the five peptides yield fragment ions that can be used to determine the amino acid sequence. The des-Arg^9 $[M+H]^+$ion does not survive activation at this collision energy and the only fragment ions that are detected are the b_2, y_2, a_4, and b_4. On the other hand, bradykinin $[M+H]^+$ ions yield an entire series of a-, b-, and y-type fragment ions, with the exception of a_3, b_3, and y_6 fragment ions. The gramicidin S SID spectrum is dominated by proline terminated fragment ions, i.e. PV (*m/z* 197), FP (*m/z* 245), PVO (*m/z* 311), LFP (*m/z* 358), PVOL (*m/z* 425), PVOLF (*m/z* 572), and PVOLFP (*m/z* 669). Similarly, the SID spectrum of substance P $[M+H]^+$ ions contains a complete sequence for b_1–b_8 and y_1–y_8 fragment ions; however, the lack of d_{10} or w_2 fragment ion does not permit distinction between the isomeric amino acid residues of leucine and isoleucine. At these collision energies we do not observe fragmentation for α-MSH.

Fig. 7 contains a series of SID mass-mobility plots for bradykinin $[M+H]^+$ ions obtained using an F-SAM surface. Spectra are shown for SID collision energies ranging from 40 to 100 eV in 20 eV increments. At 40 eV collision energies the fragmen-

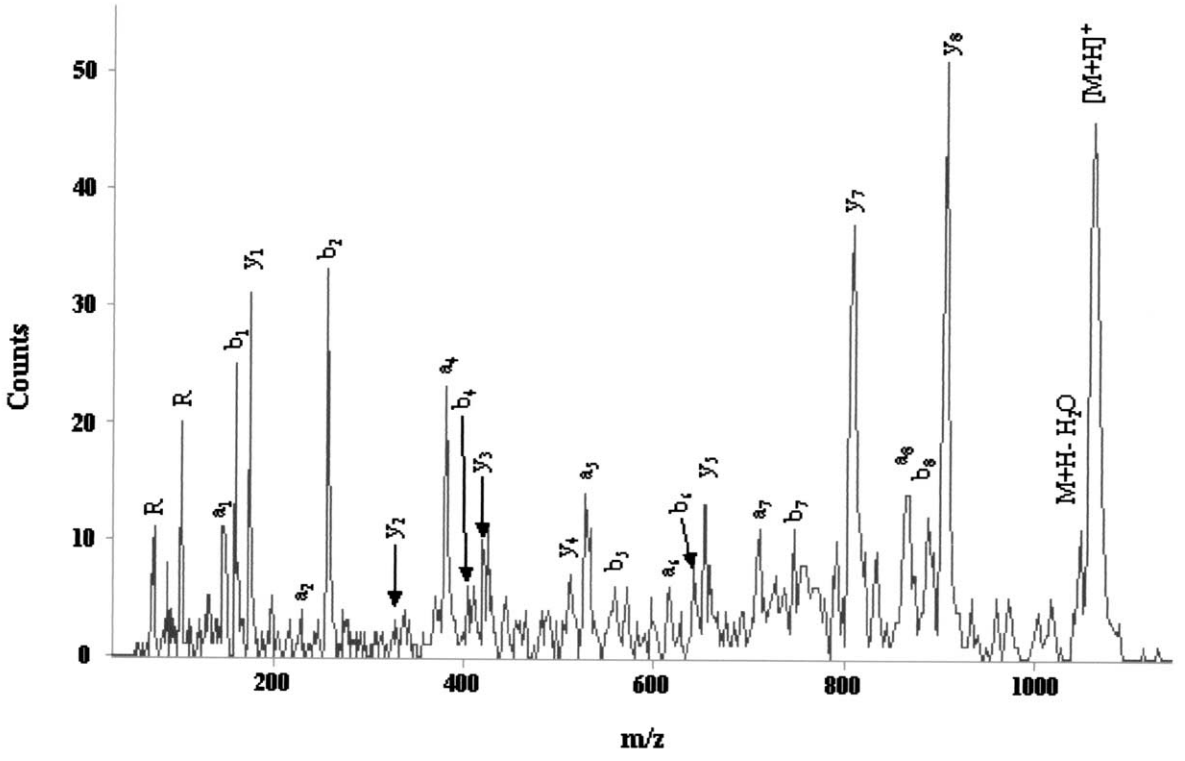

Fig. 4. A MALDI-IM-SID-o-TOF mass spectrum of bradykinin. This spectrum was acquired using the gold grid arrangement in Fig. 1, Inset A. Data was acquired for 2 min and analyzed using GRAMS/32.

tation series is incomplete and the spectrum is dominated by y_8, b_8, a_8, b_6, a_6, y_4, b_4, a_4, and y_1 fragment ions. Increasing the collision energy to 60 eV results in a more complete fragmentation series with greater individual abundances. The fragment ion abundances are very similar to that obtained for bradykinin $[M+H]^+$ ions at 90 eV collision energies from a stainless steel surface; however, the ratio of the integrated areas for the y_8 fragment ion to $[M+H]^+$ ion, is 1:1 for the F-SAM and 1:10 for the stainless steel surface. Increasing the collision energy to 80 eV increases the relative fragment ion abundances but no new fragment ions are observed and the overall mass resolution is decreased. At 100 eV collision energies, the abundances of the $[M+H]^+$ and y_8 fragment ions are reduced and low *m/z* and immonium ions dominate the spectrum. This result is consistent with the observations made by Riederer that SID fragment ion types are dependent on impact velocity [53].

The most sequence informative fragmentation appears to be observed between 40 and 60 eV collision energies for the F-SAM surface, and this is approximately a 30% reduction in collision energy relative to that for adventitious hydrocarbon-stainless steel. This observation, as well as the specific types of fragment ions produced, is consistent with claims by Miller, Callahan, and others regarding the overall value of F-SAMs for SID experiments [54,55]. In addition, the reproducibility of the SID spectra is excellent which greatly affects the analytical utility of F-SAMs for high throughput proteomic studies.

7. Evaluation of established parameters

Fig. 8 contains a mass-mobility plot for F-SAM SID of a five peptide mixture using a collision energy

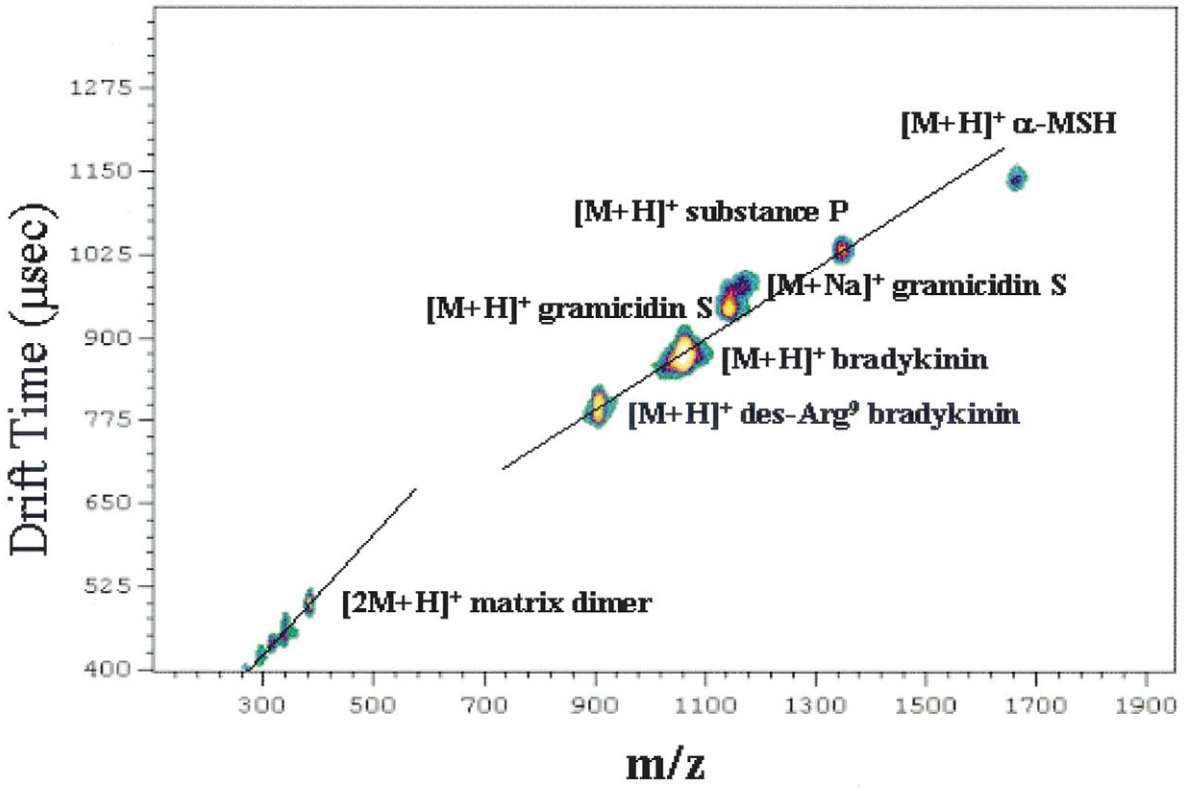

Fig. 5. A mass-mobility plot of a five-peptide mixture composed of des-Arg^9 bradykinin, bradykinin, gramicidin S, substance P, and α-MSH taken with the instrument adjusted for non-SID mass-mobility data collection. Trend lines are added as a visual aid.

of ~50 eV. Using these conditions a complete set of a-, b-, and y-type fragment ions, with the exception of a_3, b_3, and y_5, are observed for des-Arg^9 bradykinin, and similar results, a complete set of a-, b-, and y-type fragment ions, with the exception of a_3, b_3, and y_6, are observed for bradykinin. Note, however, that the abundances of the low *m/z* fragment ions are reduced with respect to those for des-Arg^9 bradykinin. The total number of fragment ions is also reduced for gramicidin S when compared to the results obtained using 90 eV collision energies and a stainless surface. The ratio of the integrated peak area of the precursor ions to the sum of the integrated peak areas of the associated fragment ions is provided in Table 1.

Fig. 9 contains an F-SAM SID mass-mobility plot obtained using a 70 eV collision energy. Only a small fraction of des-Arg^9 bradykinin $[M+H]^+$ ions survive activation, and the only SID fragment ions observed have *m/z* values of <650. This result agrees well with spectra shown in Fig. 6 for bradykinin $[M+H]^+$ ions where an increase in collision energy resulted in a depletion of the precursor ion. Similar behavior is also observed for gramicidin S, e.g. an increase in SID fragment ion abundance and a reduction in the $[M+H]^+$ ion abundance is observed as collision energy is increased. Similar results are obtained for substance P, which exhibits a near complete fragment ion series, a_1, a_2, a_5, b_1, b_2, b_4–b_8, y_1, y_3–y_8, and the usual losses of small neutrals at higher collision energies. The observed fragmentation at a 70 eV collision energy with an F-SAM surface is comparable to that observed at 90 eV (Fig. 6) using a stainless steel surface. The ratio of integrated peak area for the precursor ion to that of the SID fragment ions, listed in Table 1, is improved over that at 50 eV with an F-SAM.

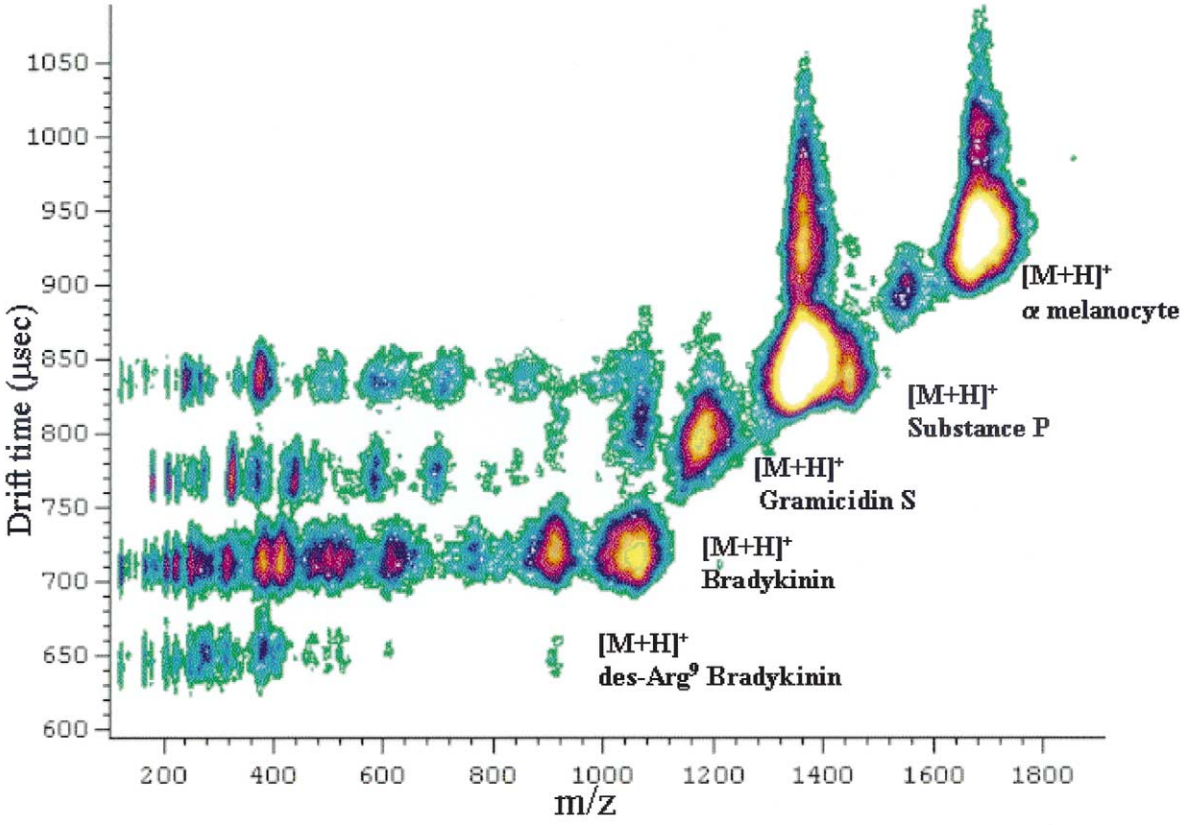

Fig. 6. Mass-mobility plot of a five-peptide mix acquired using an adventitious hydrocarbon coated stainless steel surface at ~90 eV collision energy. The correlation of fragment ions to precursor ions is illustrated.

A comparison of Figs. 6–9 underscores an important feature of SID, viz. that ions activated by SID possess a narrow distribution of internal energies. From the results shown here the use of a single collision energy appears to limit the range, ~300 *m/z*, where both the $[M+H]^+$ ion survives and sufficient sequence informative SID fragment ions are formed. It may be possible to overcome this limitation by ramping the collision voltage during the course of the experiment. In addition, instrument design may also be an important factor. For example, the F-SAM surface is positioned approximately one cm from the extraction region for these studies and there may be insufficient time for a large *m/z* ion (greater than *m/z* 1 500) to undergo dissociation. As the abundances of fragment ions observed are defined by the unimolecular dissociation rate constant which is a function of the total energy of the precursor $[M+H]^+$ ion, the critical energy of the particular fragment, and the number of vibrational modes in the precursor $[M+H]^+$ ion, it is expected that the number of vibrational modes will increase with peptide mass. This means that the fragment ion spectra is not only dependent on the internal energy deposited into the precursor $[M+H]^+$ ion and its mass, but also on the flight time from the collision surface to the extraction region of the mass spectrometer [56]. The transit time from the F-SAM surface to the extraction region 1 cm away for an *m/z* 1 500 ion having a scattered kinetic energy of 14 eV would be 4–5 μs. There may be utility for changes to the ion optics that increase arrival times for ions in the mass analyzer.

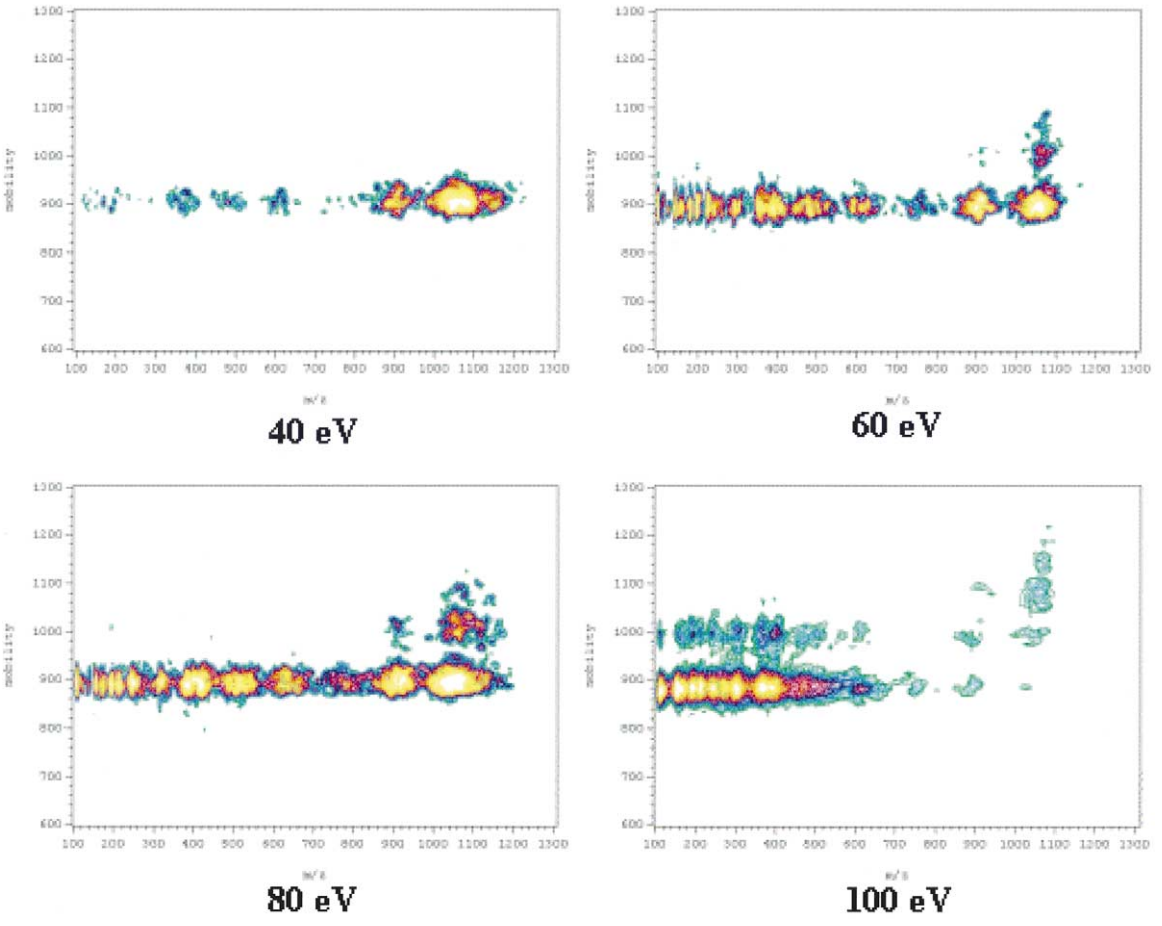

Fig. 7. Series of 2D mass-mobility plots of bradykinin at increasing collision energies (40–100 eV) with an F-SAM surface. The depletion of the precursor ion and the abundances of the fragment ions increase near linearly with collision energy.

9. Additional benefits of fluorinated self-assembled monolayers surfaces

The importance of using F-SAM surfaces for IM-SID-TOF MS is clearly illustrated by the peak tailing observed in Fig. 6. Nearly identical fragmentation patterns for protonated peptides between *m/z* 900 and 1 350 using a stainless steel at 90 eV (Fig. 6) were observed for an F-SAM at 70 eV (Fig. 9). The peak tailing observed for substance P and α-MSH using the stainless steel surface is significantly reduced for the F-SAM surface. It should be noted, however, that even with an F-SAM the choice of collision energy yields further improvements in the spectrum. That is, we see that collision energy affects peak tailing even for an F-SAM surface (see Fig. 7). By controlling the collision energy it should be possible to completely eliminate the peak tailing and thereby improve the mobility resolution.

We attribute the mobility peak tailing to “sticking” or “soft-landing” of the ions onto the surface, i.e. the ions impact the surface and some fraction of the ions reside on the surface for 10’s of microseconds and are then liberated from the surface. The amount of sticking and the time duration the ions stick to the surface appears to be a function of the nature of the surface, the nature of the impacting ion, and the collision energy. One possible explanation is that the ions

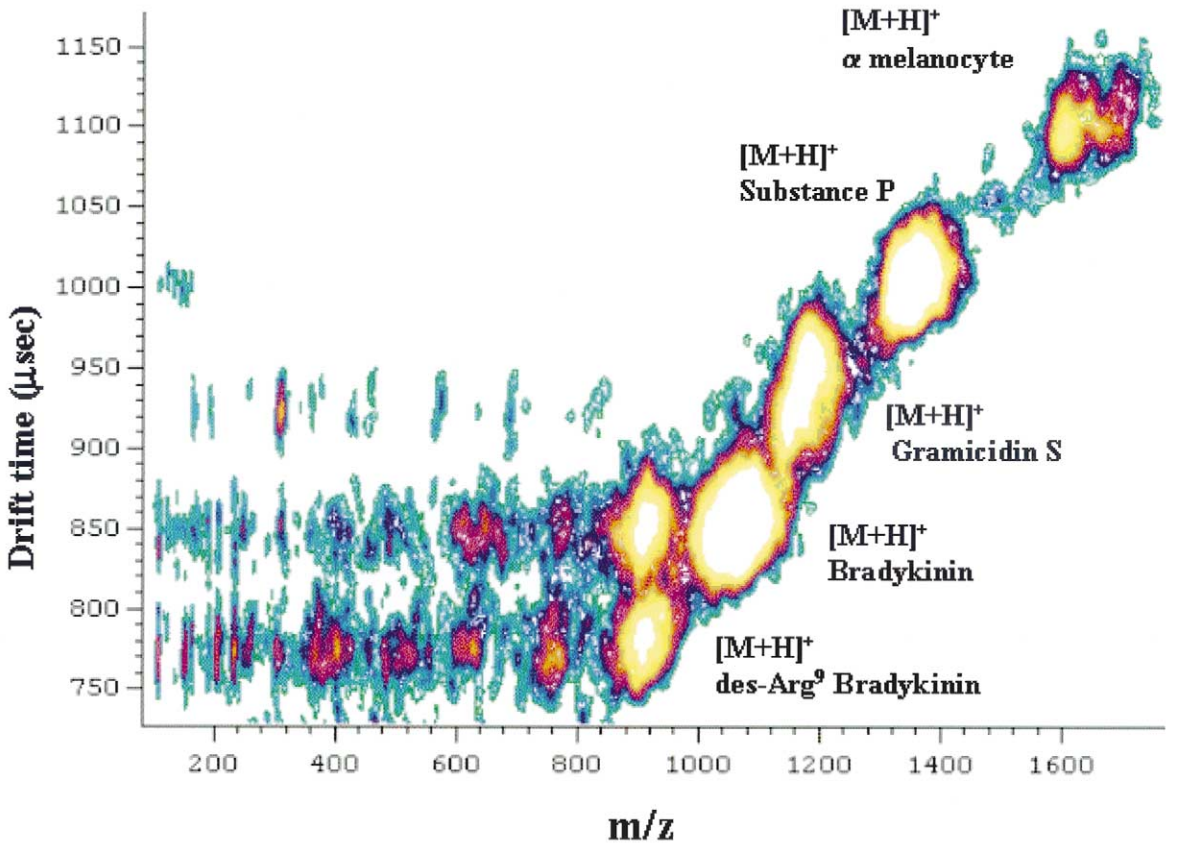

Fig. 8. Mass-mobility plot of a five-peptide mix acquired at ~50 eV collision energy with an F-SAM surface.

soft-land onto the surface and are desorbed by later arriving ions. The data shown for bradykinin precludes this possibility as there are no other ions resulting from a single laser shot and subsequent laser shots are separated by 50 ms (20 Hz repetition rate). Even at 100 eV the latest arriving ions occur approximately 300 μs after the first mobility appearance time. Another possibility is that multiply charged multimers, such as $[(M+H)_n^+]^{n+}$, are formed and upon impacting the surface the ions decompose to form $[M+H]^+$ ions. We have not ruled out this possibility; however, we have measured the arrival time distribution of bradykinin ions using high-resolution ion mobility and we do not observe multiple peaks [57]. Our preliminary conclusion is that some percentages of the colliding ions are captured by the surface and are subsequently desorbed from the surface. Investigations are underway to explore this

Table 1
Ratio of integrated area of precursor ion to the sum of integrated areas for all fragment ions

Surface/collision energy	des-Arg^9	bradykinin	gramicidin S	substance P	α-MSH
Stainless 90 eV	1:11	1:4.5	1:2.7	1.4:1	NA
F-SAM 50 eV	1:3	1:1.0	2:1.0	1:0.1	NA
F-SAM 70 eV	1:23	1:7.0	1:3.5	1:1.3	NA

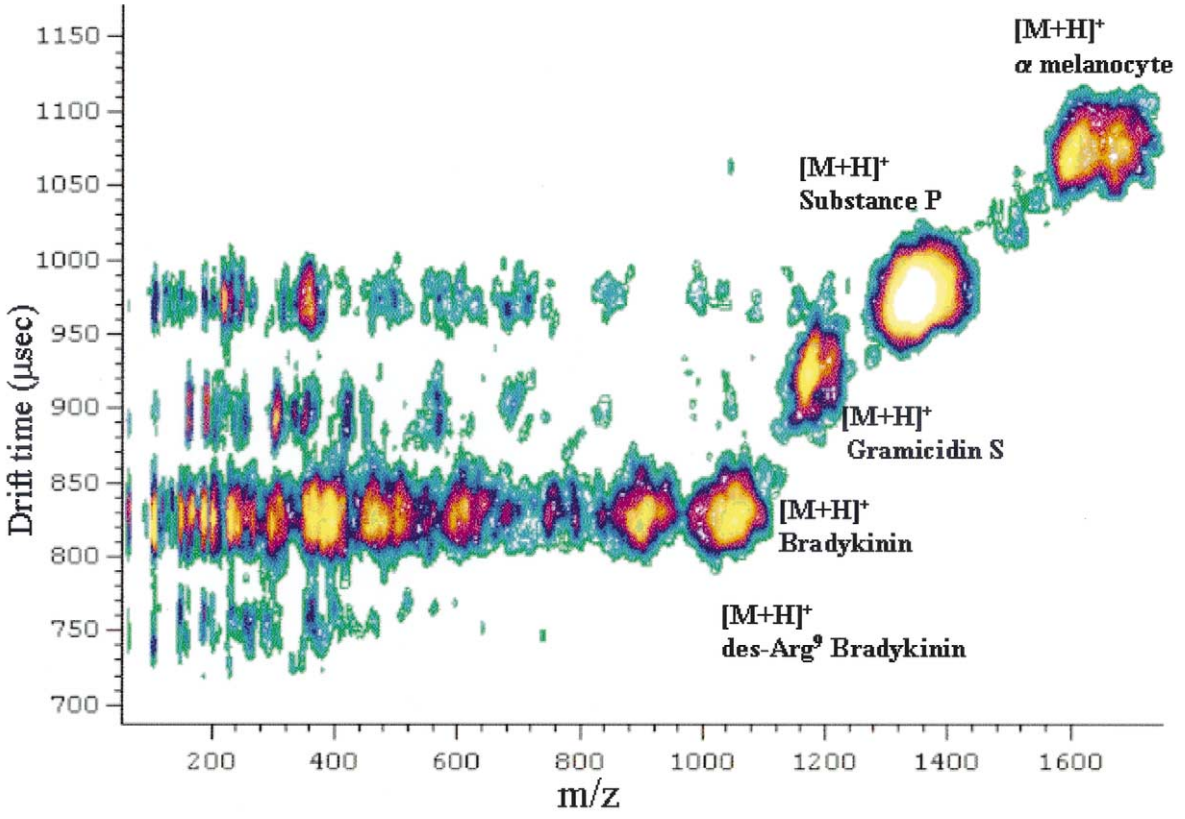

Fig. 9. Mass-mobility plot of the five-peptide mix acquired at ~70 eV collision energy with an F-SAM surface showing an improvement in signal quality over a stainless steel surface. Abundances of the most abundant fragment ions are nearly equal to the precursor ions.

further and to quantify the effects of the nature of the colliding ion with respect to the nature of the surface.

9. Conclusion

Here we demonstrate the efforts to optimize the combination of F-SAM SID and IM-TOF MS for proteomics studies. The advantage of the simultaneous acquisition of the peptide mass map and peptide sequence information is greatly facilitated by the use of F-SAM surfaces. The judicious choice of surface composition and collision energy led to significant improvements to the experiment. The implications of the technique include meeting the need for high throughput de novo sequencing of peptides and mixtures of peptides resulting from the proteolytic digest of proteins.

Acknowledgements

The TOF development research (TAMU) is supported by a grant from the U.S. Department of Energy, Division of Chemical Sciences, Basic Energy Science, and the ion mobility research (TAMU) is supported by a grant from the National Science Foundation. The Ion Mobility/TOF developmental research is supported by a NIH-SBIR grant (Ionwerks). The authors would also like to thank G. Cooks, V. Wysocki, D. Smith, and J. Laskin for helpful conversations, and V. Wysocki and D. Smith for providing the F-SAM surface used in these experiments. The authors would also like to thank T. Eagan for the data acquisition software development that expedited these results.

References

[1] A. Pandey, M. Mann, Nature 405 (2000) 837.
[2] Methods Molecular Biology, J.R. Chapman (Ed.), Humana, Totowa, New Jersey, 2000.
[3] M.J. Chalmers, S.J. Gaskell, Curr. Opin. Biotechnol. 11 (2000) 384.
[4] R. Bakhtiar, F.L.S. Tse, Mutagenesis 15 (2000) 415.
[5] R. Bakhtiar, R.W. Nelson, Biochem. Pharmacol. 59 (2000) 891.
[6] A.L. Burlingame, S.A. Carr, Mass Spectrom. Biol. Sci. (1996) 151.
[7] J.N. Selley, J. Swift, T.K. Attwood, Bioinformatics 17 (2001) 105.
[8] J.R. Yates III, Electrophoresis 19 (1998) 893.
[9] K.R. Jennings, Int. J. Mass Spectrom. 200 (2000) 479.
[10] A.K. Shukla, J.H. Futrell, J. Mass Spectrom. 35 (2000) 1069.
[11] Tandem Mass Spectrom., F.W. McLafferty (Ed.), Wiley, New York, 1983.
[12] K.J. Gillig, B.T. Ruotolo, E.G. Stone, K. Fuhrer, M. Gonin, A.J. Schultz, D.H. Russell, Anal. Chem. 72 (2000) 3965.
[13] K.M. Downard, in New Adv. Anal. Chem., Atta-ur-Rahman (Ed.), Harwood Academic Publishers, Amsterdam, Netherlands, p. 2/1.
[14] R.J. Cotter, Time-of-Flight Mass Spectrometry: Instrumentation and Applications in Biological Research, ACS, Washington, D.C., 1997.
[15] H.J. Cooper, P.J. Derrick, in NATO ASI Ser., Ser. C Mass Spectrometry in Biomolecular Sciences, R.M. Caprioli (Ed.), Kluwer Academic Publishers, London, England, 1996, Vol. 475, p. 201.
[16] D.C. Barbacci, D.H. Russell, J. Am. Soc. Mass Spectrom. 10 (1999) 1038.
[17] B. Spengler, D. Kirsch, R. Kaufmann, Rapid Commun. Mass Spectrom. 5 (1991) 198.
[18] V. Grill, J. Shen, C. Evans, R.G. Cooks, Rev. Sci. Instrum. 72 (2001) 3149.
[19] L. Lingjun, C. Masselon, G.A. Anderson, T.P. Conrads, K. Alving, L. Pasa-Tolic, T.D. Veenstra, R.D. Smith, Proceedings of the 2001 Pittsburgh Conference, New Orleans, LA, March 2001 .
[20] M. Karas, U. Bahr, in NATO ASI Ser., Ser. C Mass Spectrometry in Biomolecular Sciences, R.M. Caprioli (Ed.), Kluwer Academic Publishers, London, England, 1996, Vol. 475, p. 33.
[21] R. Zenobi, R. Knochenmuss, Mass Spectrom. Rev. 17 (1999) 337.
[22] Time-of-Flight Mass Spectrometry: Instrumentation and Applications in Biological Research, R.J. Cotter (Ed.), ACS, Washington, D.C., 1997.
[23] G.R. Kinsel, L.M. Preston, D.H. Russell, Biol. Mass Spectrom. 23 (1994) 205.
[24] Laser Ionization Mass Analysis [In: Chemical Analysis 124], A. Vertes, R. Gijbels, F. Adams (Eds.), Wiley, New York, 1993.
[25] E. Denisov, J. Laskin, A. Shukla, J. Futrell, Proceedings of the 49th ASMS Conference on Mass Spectrometry and Allied Topics, Chicago, IL, 2001.
[26] F.H. Strobel, T. Solouki, M.A. White, D.H. Russell, J. Am. Soc. Mass Spectrom. 2 (1991) 91.
[27] T. Laurell, J. Nilsson, G. Marko-Varga, J. Chromatogr., B: Biomed. Sci. Appl. 752 (2001) 217.
[28] J. Preisler, P. Hu, T. Rejtar, B.L. Karger, Anal. Chem. 72 (2000) 4785.
[29] B.T. Ruotolo, K.J. Gillig, E.G. Stone, D.H. Russell, Int. J. Mass Spectrom., submitted.
[30] B.T. Ruotolo, K.J. Gillig, E.G. Stone, Z.-Y. Park, D.H. Russell, Proceedings of the 48th ASMS Conference on Mass Spectrometry and Allied Topics, Long Beach, CA, 2000.
[31] J.A. Ragas, T.A. Simmons, P.A. Limbach, Analyst 125 (2000) 575.
[32] Z.-Y. Park, D.H. Russell, Anal. Chem. 73 (2001) 2558.
[33] R.D. Bagshaw, J.W. Callahan, D.J. Mahuran, Anal. Biochem. 284 (2000) 432.
[34] G.A. Eiceman, Z. Karpas, Ion Mobility Spectrometry, CRC, Boca Raton, FL, 1994.
[35] R.H. St. Louis, H.H. Hill Jr., Crit. Rev. Anal. Chem. 21 (1990) 321.
[36] E.G. Stone, K.J. Gillig, B.T. Ruotolo, K. Fuhrer, M. Gonin, A.J. Schultz, D.H. Russell, Anal. Chem. 73 (2001) 2233.
[37] C.S. Hoaglund-Hyzer, J. Li, D.E. Clemmer, Anal. Chem. 72 (2000) 2737.
[38] C.S. Hoaglund-Hyzer, D.E. Clemmer, Anal. Chem. 73 (2001) 177.
[39] C.D. Bradley, J.M. Curtis, P.J. Derrick, M.M. Sheil, J. Chem. Soc., Faraday Trans. 90 (1994) 239.
[40] D.L. Bricker, D.H. Russell, J. Am. Chem. Soc. 108 (1986) 6174.
[41] R.G. Cooks, S.A. Miller, in NATO ASI Ser., Ser. C Fundamentals and Applications of Gas Phase Ion Chemistry, K.R. Jennings (Ed.), Kluwer Academic Publishers, London, England, 1999, Vol. 521, p. 55.
[42] A. Somogyi, T.E. Kane, J.M. Ding, V.H. Wysocki, J. Am. Chem. Soc. 115 (1993) 5275.
[43] V.J. Angelico, S.A. Mitchell, V.H. Wysocki, Anal. Chem. 72 (2000) 2603.
[44] M.E. Bier, J.W. Amy, R.G. Cooks, J.E.P. Syka, P. Ceja, G. Stafford, Int. J. Mass Spectrom. Ion Processes 77 (1987) 31.
[45] E.A. Mason, E.W. McDaniel, in Transport Properties of Ions in Gases, Wiley, New York, 1988, p. 442.
[46] D.E. Clemmer, M.F. Jarrold, J. Mass Spectrom. 32 (1997) 577.
[47] J.A. Loo, C.G. Edmonds, R.D. Smith, Anal. Chem. 65 (1993) 425.
[48] S.J. Shields, B.K. Bluhm, D.H. Russell, J. Am. Soc. Mass Spectrom. 11 (2000) 626.
[49] A.R. Dongre, A. Somogyi, V.H. Wysocki, J. Mass Spectrom. 31 (1996) 339.
[50] M. Mak, G. Mezo, Zs. Skribanek, F. Hudecz, Rapid Commun. Mass Spectrom. 12 (1998) 837.
[51] K.J. Gillig, D.H. Russell, in preparation.
[52] Plasma Chromatography, T.W. Carr (Ed.), Plenum, New York, 1984.
[53] D.E. Riederer, L.L. Haney, A.R. Hilgenbrink, J.R. Beck,

Proceedings of the 48th ASMS Conference on Mass Spectrometry and Allied Topics, Long Beach, CA, 2000.
[54] S.A. Miller, H. Luo, X. Jiang, H.W. Rohrs, R.G. Cooks, Int. J. Mass Spectrom. Ion Processes 160 (1997) 83.
[55] J. H. Callahan, A. Somogyi, V.H. Wysocki, Rapid Commun. Mass Spectrom. 7 (1993) 693.
[56] T. Baer, W.L. Hase, Unimolecular Reaction Dynamics, Theory and Experiments, Oxford University Press, New York, 1996.
[57] A.E. Counterman, S.J. Valentine, C.A. Srebalus, S.C. Henderson, C.S. Hoaglund, D.E. Clemmer, Am. Soc. Mass Spectrom. 9 (1998) 743.